Internal Dynamics of Green Fluorescent Protein

Volkhard Helms,*,†,‡ T. P. Straatsma,§ and J. Andrew McCammon†

Department of Chemistry and Biochemistry, and Department of Pharmacology, University of California at San Diego, 9500 Gilman Drive, La Jolla, California 92093-0365, and Theory, Modeling and Simulation, Environmental Molecular Science Laboratory, Pacific Northwest National Laboratory, Battelle Blvd., MS KI-96, Richland, Washington 99352

Received: July 22, 1998; In Final Form: December 2, 1998

A 1 ns molecular dynamics simulation was performed to study the dynamic behavior of wild-type green fluorescent protein from *Aequorea victoria*. We find the protein to be remarkably rigid, both overall, because the cylindrical β-barrel provides a stable framework, but also on an atomic level in the immediate surrounding of the chromophore. Here, a tight H-bond network is formed mainly involving six internal water molecules. The perfect barrel is interrupted only between β-strands 7 and 8 where contact is made via side chain interactions, and we investigated the dynamic behavior of this region in detail. After ca. 320 ps of simulation, an arginine residue, initially sticking out into solution, folded over the cleft to form a H-bond with a backbone oxygen atom on the opposite strand. This contact appears important for stabilization of the overall protein architecture.

Introduction

Green fluorescent protein (GFP) has become a unique tool in molecular biology in recent years as a protein marker in living cells, easily detectable by fluorescence spectroscopy.[1] The general shape of the protein, as determined by X-ray crystallography,[2,3] is sketched in Figure 1. A cylinder of roughly 40 Å length and 30 Å diameter is formed by 11 β-strands lining up to form a nearly perfect β-barrel. A central helix runs through the cylinder, containing the chromophore. The top and bottom of the cylinder are covered by short helices and loops. The buried chromophore is formed by a posttranslational cyclization of the polypeptide backbone, involving residues Ser65, Tyr66, and Gly67.[4] It has been shown that the β-barrel folds first.[5] Cyclization of the chromophore then occurs in the rigid GFP framework which causes a strained conformation of the central helix. The excitation spectrum indicates very little quenching of the excited state by O_2.[6] The structure seems to provide a perfect scaffold to protect the buried chromophore from the environment.

The ideal symmetry of the β-barrel is broken only at one location,[7] between strands 7 and 8 (see Figure 2). Here, connections are made by side chain contacts between opposite pairs of hydrophobic residues (Val 150−Phe165 and Ile 152−Val163), a H-bond between His148:NE2 and Arg168:N, and by polar interactions between a cluster of three asparagine residues (Asn 144, 146, and 170). The nonregularity of the β-barrel may be necessary to allow for protein folding. To investigate the overall mobility of the protein and the nonregularity in particular, we have performed a 1 ns simulation of wild-type GFP with its chromophore in the neutral state solvated in a periodic solvent box. The system was simulated at constant pressure, and long-range electrostatic interactions were included via a Particle-Mesh-Ewald method.[8]

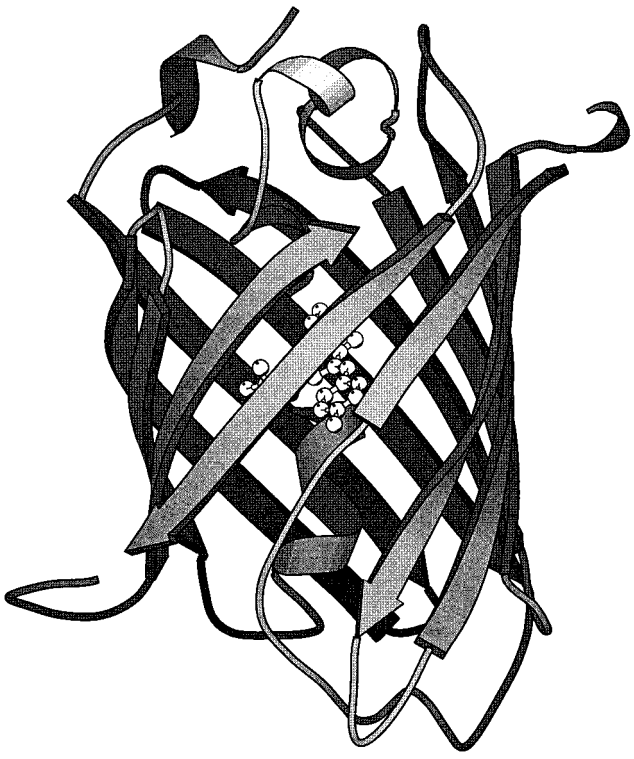

Figure 1. Schematic view of the secondary structure of green fluorescent protein.[9] The chromophore is shown in atomic detail in white. The figure was produced with MOLSCRIPT.[32]

Methods

The coordinates of wild-type GFP were taken from the Protein Data Bank entry 1emb.pdb. This structure contains a Gln to Arg mutation at position 80 and was determined at 2.1 Å

* Corresponding author.
† University of California at San Diego.
‡ Current address: Max-Planck-Institute of Biophysics, Kennedyallee 70, 60596 Frankfurt, Germany. Tel: +1 (69) 6303−202. Fax: +1 (69) 6303-251. e-mail: vhelms@biophys.mpg.de.
§ Pacific Northwest National Laboratory.

10.1021/jp983120q CCC: $18.00
Published on Web 04/02/1999

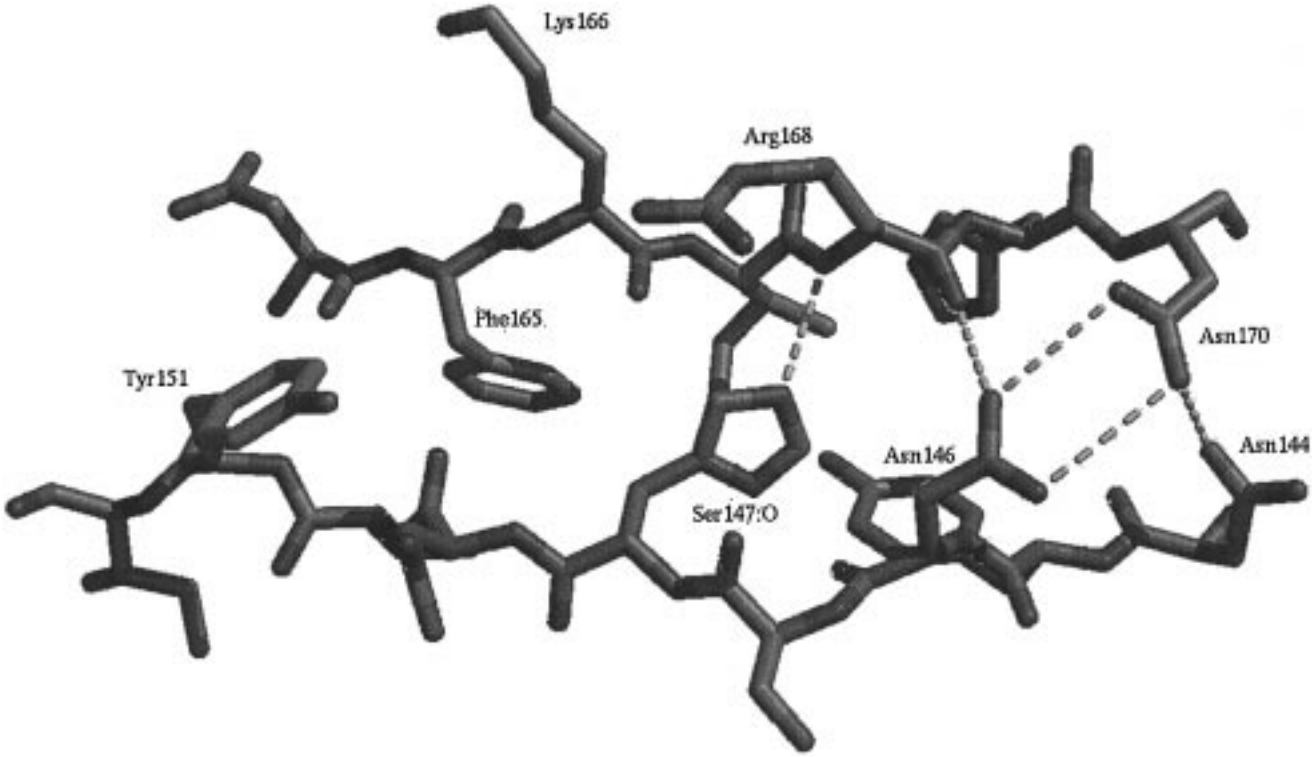

Figure 2. Cleft between β-strands 7 and 8. Dashed lines indicate possible H-bonds between side chain atoms of both strands. The figure was produced using the MidasPlus program.[33,34]

resolution.[9] The first residue and the nine last ones were not visible in the crystal structure and were therefore omitted from the simulation. The N-terminus of Ser2 and C-terminus of Ile229 were treated as charged. Besides the 74 original crystal waters, two additional water molecules were added in vicinity to the chromophore because they are contained in the S65T crystal structure as WAT383 and WAT320, and one of them was also found in an independently determined crystal structure of GFP wild-type[2] as WAT255. The protonation states of histidine residues were assigned by visual inspection of their surroundings (His 77, 81, 139, and 169 are protonated at N_ϵ, all others at N_δ). Polar hydrogens were added using the HB2MAK routine[10] of the WHATIF program,[11] and apolar hydrogens with the INSIGHT program.[12] To achieve overall neutrality of the system, six Na^+ counterions were placed, roughly evenly spaced, in energetically favorable positions on the protein surface that were identified with the GRID program.[13] To derive partial atomic charges, a model chromophore was constructed consisting of the two aromatic rings. The Ser65 portion of the chromophore was replaced by a methyl group. An ab initio geometry optimization of the model chromophore was then performed with the GAMESS program[14] up to the RHF/6-31G-(d) level.[15] Partial atomic charges for the chromophore atoms in the two aromatic rings were calculated from an electrostatic potential fit,[16] while partial charges for the atoms of the Ser portion were taken from the AMBER94 force field[17] as well as those for the linking atoms to Val64. Geometric constants were taken from the ab initio optimized geometry, and covalent force constants and van der Waals parameters for the chromophore were assigned in analogy with AMBER94.

The protein was then solvated in a cubic box with dimensions of 69 Å, so that each protein atom was at least at 8 Å distance from the box edges. The systems contained 3583 solute atoms, and 9381 water molecules, a total of 31 726 atoms. Energy minimizations and molecular dynamics simulations were performed with the NWChem program[18] using the AMBER94 force field on the parallel Cray T3E of the San Diego Supercomputing Center. Short-range nonbonded interactions were calculated up to a 10 Å cutoff. Long-range electrostatic interactions were treated by the Particle-Mesh-Ewald method[8] using a 64^3 grid, and periodic boundary conditions were used. The bond-lengths between hydrogens and bonded heavy atoms were constrained by the SHAKE algorithm.[19] A 2 fs time step was used. The temperature of solute and solvent was controlled by separately coupling them to Berendsen thermostats[20] with coupling constants of 0.1 and 0.4 ps. The system was equilibrated in the following way: (a) the positions of all atoms were optimized by 1000 steps of steepest descent energy minimization, (b) the solvent was equilibrated during 20 ps MD simulation at 300 K at constant temperature and pressure (NPT) while the protein was kept fixed, (c) the protein part was slowly heated during 5 ps MD simulations at 50 K, 100 K, ..., 300 K at constant energy and volume while velocities were reassigned every 500 steps and solvent molecules were kept fixed, (d) 10 ps simulation of the whole system at 300 K without velocity reassignment, and (e) 1 ns simulation of the whole system under NPT conditions. Equilibration was checked by monotoring the individual energy components. The last 0.9 ns were used for data collection.

Numerical analysis of the trajectories was performed with the WHATIF program.[11] Animation of the trajectory was performed with the INSIGHT program[12].

Results

Stability of the Cylindrical β-Barrel. The RMS deviation of the backbone atoms from their positions in the crystal structure remains approximately constant at around 0.9 Å during the 1 ns molecular dynamics simulation, see Figure 3, and seems to have reached a stable plateau. Figure 4 displays a comparison of atomic RMS fluctuations during the simulation with crystallographic B-factors. Although the MD data has a lower base level, the maxima are obtained at exactly the same locations.

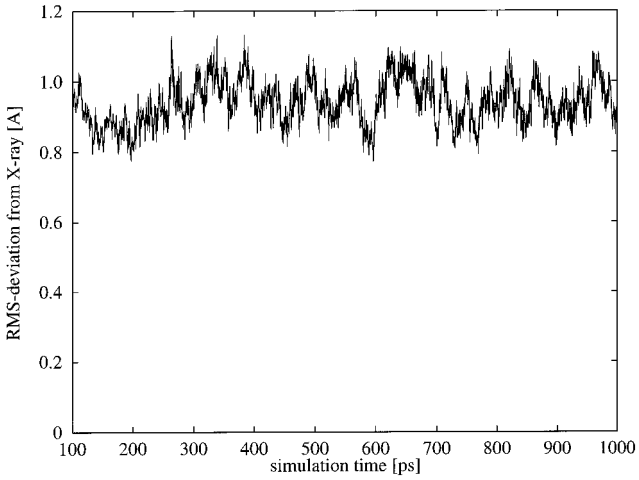

Figure 3. RMS deviation of C_α-atoms from X-ray conformation during the molecular dynamics simulation. Data are from the last 0.9 ns of the simulation.

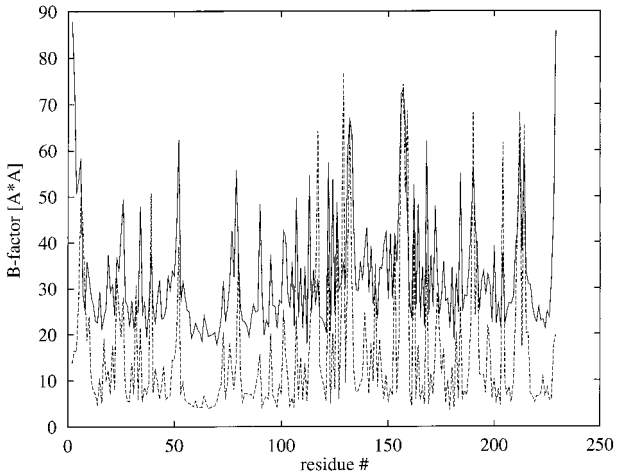

Figure 4. Atomic RMS fluctuations during the MD simulation averaged per residue are converted into simulated B-factors (dashed line) and compared to the crystallographic B-factors (straight line).

To extract important low-frequency fluctuational modes of the protein, an "essential dynamics analysis" of the trajectory[21] was performed. The projection of the trajectory onto the first three eigenvectors is shown in Figure 5. Obviously, the β-barrel is hardly moving at all. Noticeable motion occurs only in the loop segments between β-strands. To ensure that this behavior is independent of solvent effects, we computed the diffusion coefficient of the surrounding bulk solvent molecules ($2.5 \pm 0.1 \times 10^{-9}$ m s^{-2}). This value compares very well to that of bulk SPC/E water[22] (2.7×10^{-9} m s^{-2}) and to an experimental value[23] at standard conditions (2.4×10^{-9} m s^{-2}). The stability of the protein cylinder was also analyzed by monitoring the occupancy of backbone−backbone H-bonds between adjacent β-strands. Figure 6 shows a schematic representation. Most of these H-bonds actually have occupancies higher than 90%. The imperfection of the β-barrel between strands 7 and 8 is apparent in the center of Figure 6. Graphical analysis of coordinate frames at regularly spaced intervals showed no water access to the cylinder interior.

Hydrogen-Bond Network Involving Chromophore. Hydrogen-bond occupancies of residues in the surrounding of the chromophore are shown in Figure 7. On average, the six water molecules are involved in 2 to 3 H-bonds. Wat 1 alternates between four very close contacts. Wat 2 appears to be locked in in a favorable static configuration, and very efficiently stabilizes the hydroxyl oxygen of Thr203. The two added water molecules 5 and 6 are the most flexible ones; they adopt multiple orientations. Furthermore, Wat 5 forms the least number of H-bonds on average (ca. 2). These observations may explain why these two water molecules were not assigned in the crystallographic determination.[9] Overall, the H-bond network appears very tight. For example, the H-bonds along the chain Cro:OH−Wat−Ser205−Glu222−Cro:OG all have occupancies in the range between 80 and 100%. The chromophore geometry is almost planar throughout the simulation. The two dihedrals N2−CA2−CB2−CG2 and CA2−CB2−CG2−CD1 along the ring-bridging central bonds of the chromophore display values of 2.1 ± 6.1 ° and of 2.1 ± 7.7 °.

Dynamics of Residues at the Cleft Interface. Table 1 lists distances between atom pairs from opposite sides of the cleft for various GFP crystal structures and the average distance in the molecular dynamics simulation. In general, there is good agreement among the different crystal structures and with the distances from the simulation. An important result from the simulation is that the H-bonds between the cluster of asparagine residues and with Arg168 are not constantly maintained due to competing solvent molecules as shown by their average values between 3.4 and 3.7 Å and the large RMS fluctuations. These

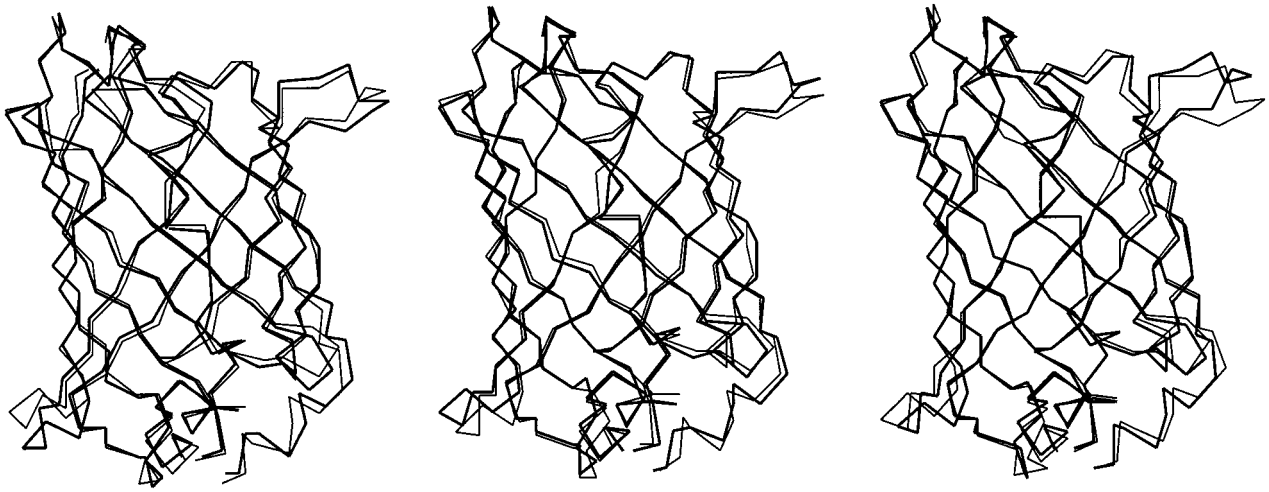

Figure 5. Projection of molecular dynamics trajectory onto eigenvectors obtained from an essential dynamics analysis.[21] The maximal (thick lines) and minimal amplitudes (thin lines) are shown for the largest eigenvalue (left), second-largest (middle), and third-largest (right). The figure was produced with INSIGHT.[12]

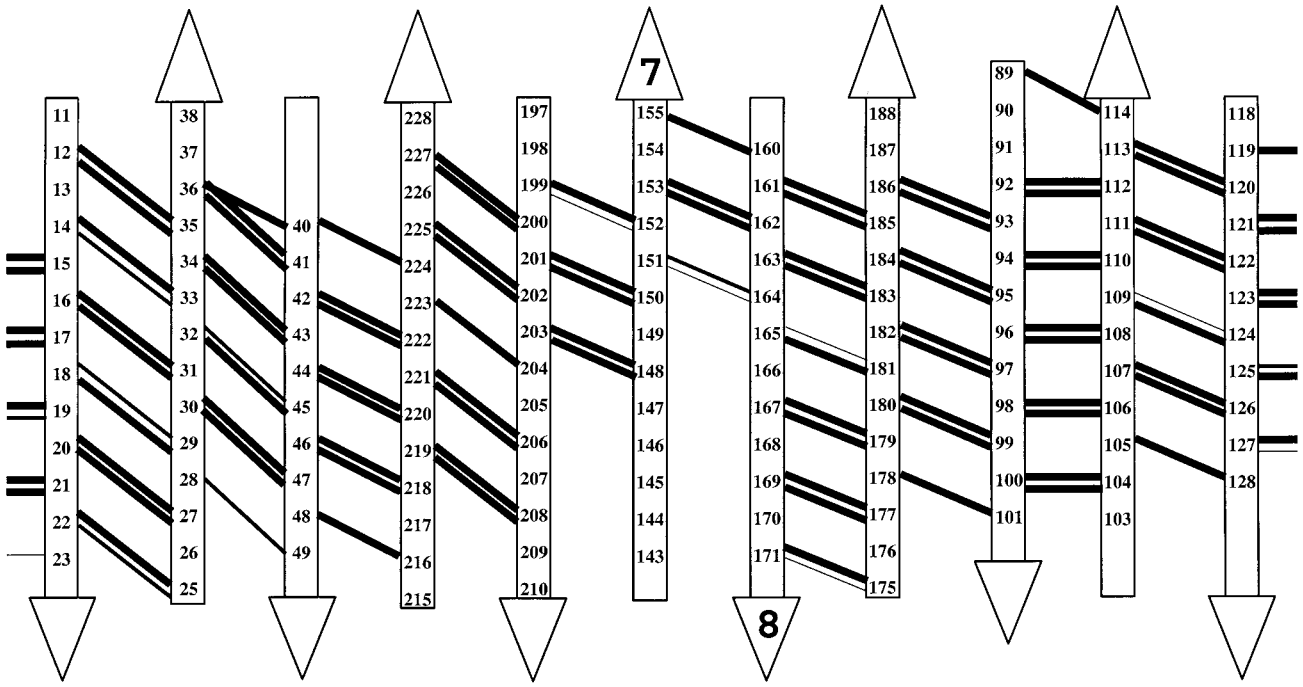

Figure 6. Schematic representation of the occupancy of backbone−backbone H-bonds of the GFP β-barrel during a 1 ns simulation of GFP wild-type with a neutral chromophore. Arrangement of strands and residue labeling follow the one in ref 3. Thick lines indicate well-preserved H-bonds with occupancies higher than 80%, normal lines indicate H-bonds of intermediate strength (60−80% occupancy), and thin lines indicate weak H-bonds (<60% occupancy).

TABLE 1: Distances (Å) between Atom Pairs on Opposite Sides of the Cleft between Strands 7 and 8 in GFP Crystal Structures of the Wild-Type by the Remington Group[9] (1emb), a S65T Single Mutant[3] (1ema), Wild-Type by the Phillips Group[2] (1gfl), and a F64L I167T K238N Triple Mutant by the Wlodawer Group[28] (1emc)[a]

	1emb	1ema	1gfl (A)	1emc (A)	MD
Met153:N−Lys162:O	3.09	2.98	2.87	2.81	3.11 ± 0.23
Tyr151:O−Asn164:N	3.49	3.10	3.06	3.34	3.26 ± 0.30
Tyr151:N−Asn164:O	3.73	3.08	3.14	3.34	3.93 ± 0.49
Asn149:O−Phe165:CB	3.78	3.42	3.44	3.51	3.86 ± 0.33
Asn149:O−Lys166:N	5.50	5.12	5.28	5.19	5.45 ± 0.34
His148:CB−Lys166:O	4.45	4.48	4.44	4.23	4.98 ± 0.43
His148:NE2−Arg168:N	3.19	3.18	2.94	3.30	3.13 ± 0.17
Asn146:ND2−Asn168:O	3.14	2.73	2.80	2.82	3.69 ± 1.35
Asn146:ND2−Asn170:OD1	3.51	3.43	3.28	3.24	3.43 ± 0.93
Asn146:OD1−Asn170:ND2	3.94	3.84	3.71	3.76	3.68 ± 0.76

[a] T167 in 1emc is not involved in intra-strand connections. For 1gfl and 1emc, subunit A was used. The last column contains averages and standard deviations of the values obtained from the MD trajectory.

distances had typical lengths of H-bonds (distance shorter than 3.5 Å) only during 75% (Asn146:ND2−ASN170:OD1), 69% (Asn146:ND2−Arg168:O), and 52% (Asn146:OD1−Asn170:ND2) of the simulation time.

Arg168 Movement. The two strands 7 and 8 are connected via a H-bond between His148:ND and Arg168:N. The S65T crystal structure[3] and the wild-type crystal structure of Phillips and co-workers[2] also contain a H-bond between Arg168 and Ser147:O where Arg168 folds over His148. However, in the wild-type structure of Remington and co-workers[9] that was used as starting structure for this study, Arg168 sticks out into solution. We observed that after 318 ps of simulation, Arg168 folded back onto the protein surface to form a H-bond with Ser147, just as is observed in the other structures. The time evolution of the distance between the two nitrogen atoms of Arg168 and the Ser147 backbone oxygen atom is shown in Figure 8. A bifurcated H-bond involving NH1 and NH2 is formed at ca. 400 ps simulation time. During most of the time, however, only NH2 is involved in H-bond formation. The critical event for H-bond formation is rotation around the $\chi 3$ angle as shown in Figure 9. The H-bonded situation is stable for ca. 200 ps. Figure 10 shows a series of six snapshots that illustrate this event. Within 0.4 ps, the side chain of Arg168 rotated around $\chi 3$. Another 1.6 ps later, its charged guanidinium group was loosely connected to Ser147:O at a distance of ca. 3.5−4 Å. Finally, after another 8 ps, the two groups formed a tight H-bond that was maintained during 67% of the remaining simulation time.

Discussion

Why proteins with different functions are folded into a variety of distinct folds is a very important field of research. In the case of GFP, an obvious function of its cage-like cylinder is to protect the chromophore from the solvent environment. In this study, a molecular dynamics simulation was used to create a realistic picture of the mobility that such a cylindrical protein exhibits on a 1 ns time scale. Certainly, reorientation of individual water molecules, formation and disruption of H-bonds and salt bridges, and even rearrangments of H-bond networks involving a number of protein groups are possible on this time scale, and have been observed in previous protein simulations.[24]

One referee pointed out that omission of more than seven C-terminal residues leads to a total loss of GFP fluorescence experimentally that may be attributed either to reduced protein stability or to alteration of the protein structure.[25] Although this is certainly a valid point of concern, it is very unlikely that protein unfolding or structural transitions will occur during a 1 ns MD simulation at room temperature. Moreover, we do not address the stability of GFP but the flexibility or rigidity of its architecture. The simulated dynamics of the shortened GFP, especially in the chromophore core region, will resemble closely that of the fully intact protein. In the simulation of GFP in a periodic solvent box, the positions of the backbone atoms during

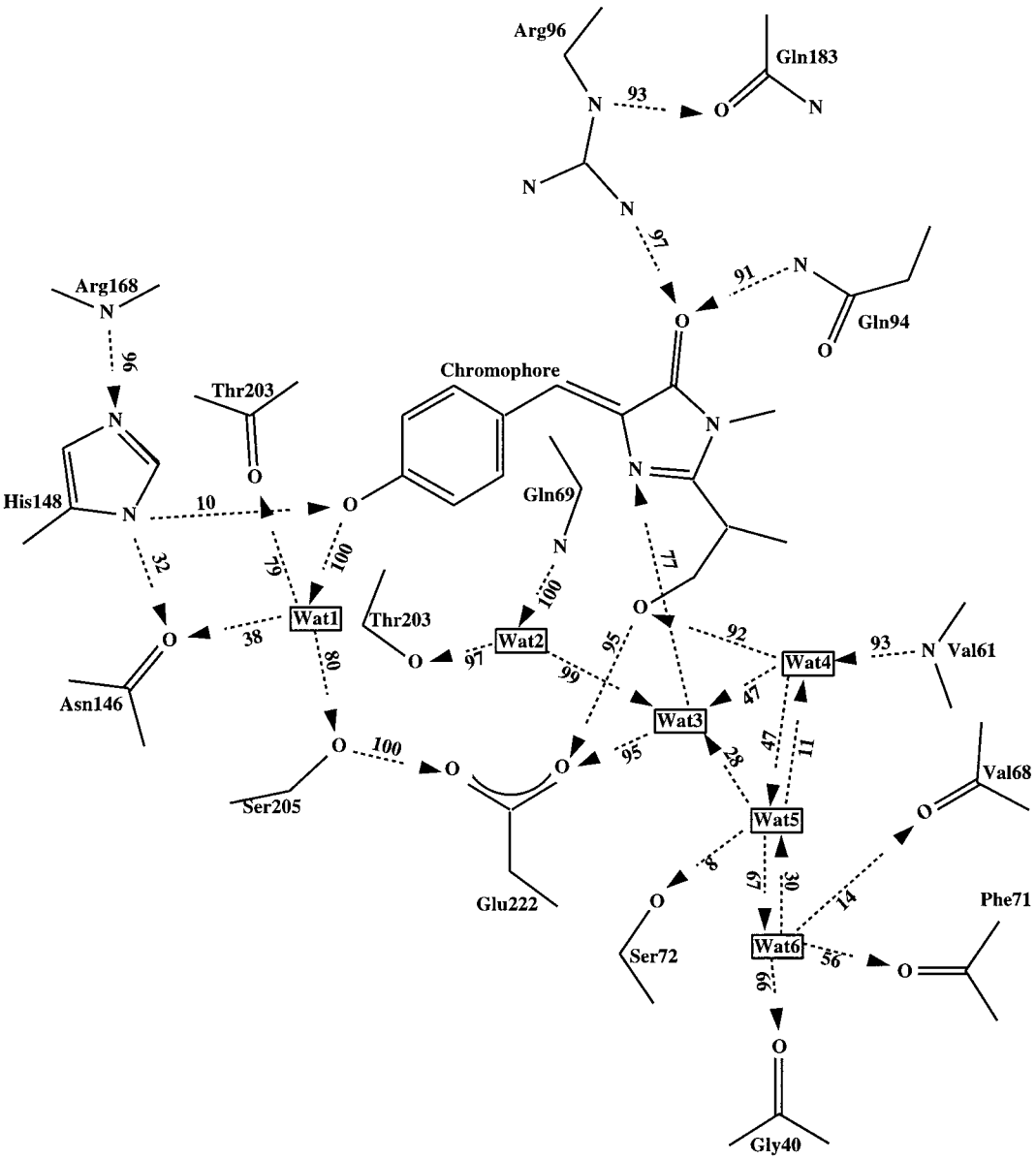

Figure 7. H-bond network in the immediate surrounding of the chromophore. H-bond occupancies during the MD simulation are given in percent. Arrows point from donor to acceptor atoms.

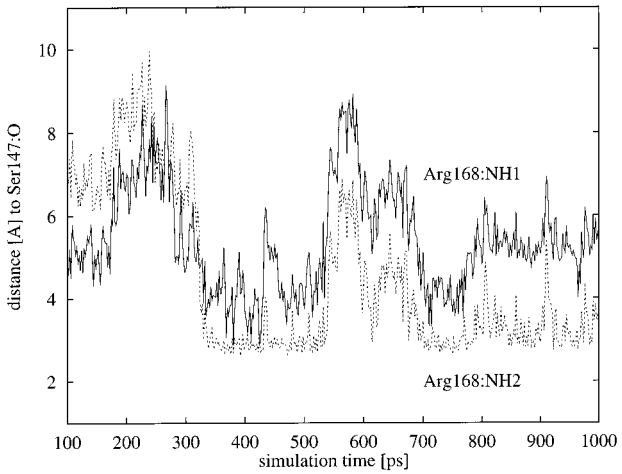

Figure 8. Time evolution of the distances between Arg168:NH1 and NH2 and the backbone oxygen of Ser147 located in the opposite strand.

the simulation deviate on average only by 0.9 Å from their crystal positions. A similarly low value (1.13 Å for all backbone atoms) was previously obtained in a 1.2 ns MD simulation of the 76 residue protein ubiquitin, also using the Amber94 force field and a Particle-Mesh-Ewald (PME) method.[26] The RMS deviation of all heavy atoms from their crystal positions is ca. 1.4 Å. Only very few protein simulations employing a similar treatment of long-range electrostatic forces have been published to date. We expect that proteins with considerable internal flexibility will exhibit RMS deviations of backbone atoms from crystal structures of ca. 1.5 Å when PME or comparable methods are used.

Together with the results from an essential dynamics analysis, and from monitoring the H-bond occupancies of the β-barrel backbone and of the chromophore surrounding, we obtain for GFP the picture of a remarkably rigid protein. How can this be interpreted in the light of experimental data? The rigid nature of GFP clarifies the origin of the high fluorescence quantum yield of GFP; steric clashes with the protein environment found in the simulation presumably can suppress possible isomerization of the chromophore and also serve to reduce possible loss of electronic excitation through vibrational energy transfer to the protein solvent shell. Indeed, the chromophore in solution is

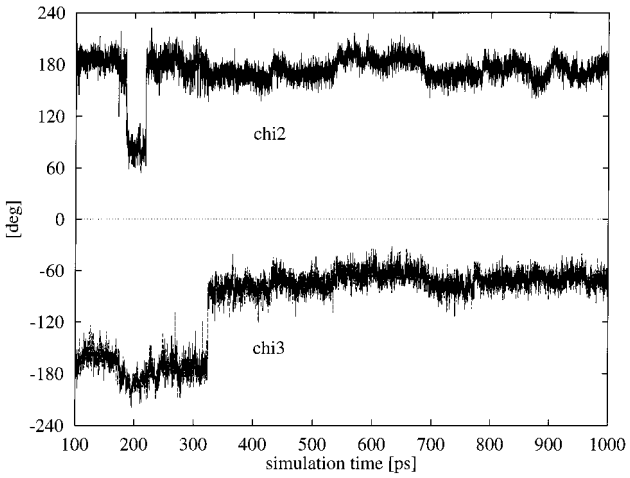

Figure 9. Time evolution of two dihedral angles of the Arg168 side chain. $\chi 2$ displays a short transition around 200 ps, but this does not affect the distance toward Ser147 (compare Figure 7). However, rotation around $\chi 3$ at ca. 320 ps is followed by contact formation between both residues.

not significantly fluorescent at room temperature,[27] underscoring the importance of the protein solvent shell in providing stabilization. The rigid framework of the protein barrel also serves as a natural protection of the GFP fluorescence signal against external influences such as quenching by molecular oxygen.[7] The rigidity is not only observed on a global scale, but also extends into the immediate chromophore environment where six water molecules are locked into "ice-like" positions through a tight H-bond network and oppose isomerization of the chromophore. In particular, one water molecule donates a strong H-bond to the hydroxyl group of Thr203. Different rotameric states of Thr203 are believed to be the main structural difference between two states of wild-type GFP where the chromophore is either found in a neutral or in an anionic form.[9,28] Formation of this H-bond may therefore be important for the stabilization of neutral chromophore in wild-type GFP.

The structure of GFP contains a very interesting irregularity of the β-barrel between strands 7 and 8 that may be crucial for folding and unfolding of the protein. Also, since the GFP fluorescence signal is quite sensitive to external pH,[29,30] this region may be important for allowing proton access to and from the chromophore region. By knowing which interactions hold the two strands together, it may be possible to design protein mutations that either strengthen or weaken the linkage between both strands. A cluster of three asparagine residues seems to form strong polar connections in various crystal structures of GFP. However, our simulation shows that, in solution, the H-bonds between these residues are shared with solvent molecules because all residues are all fully solvent exposed.

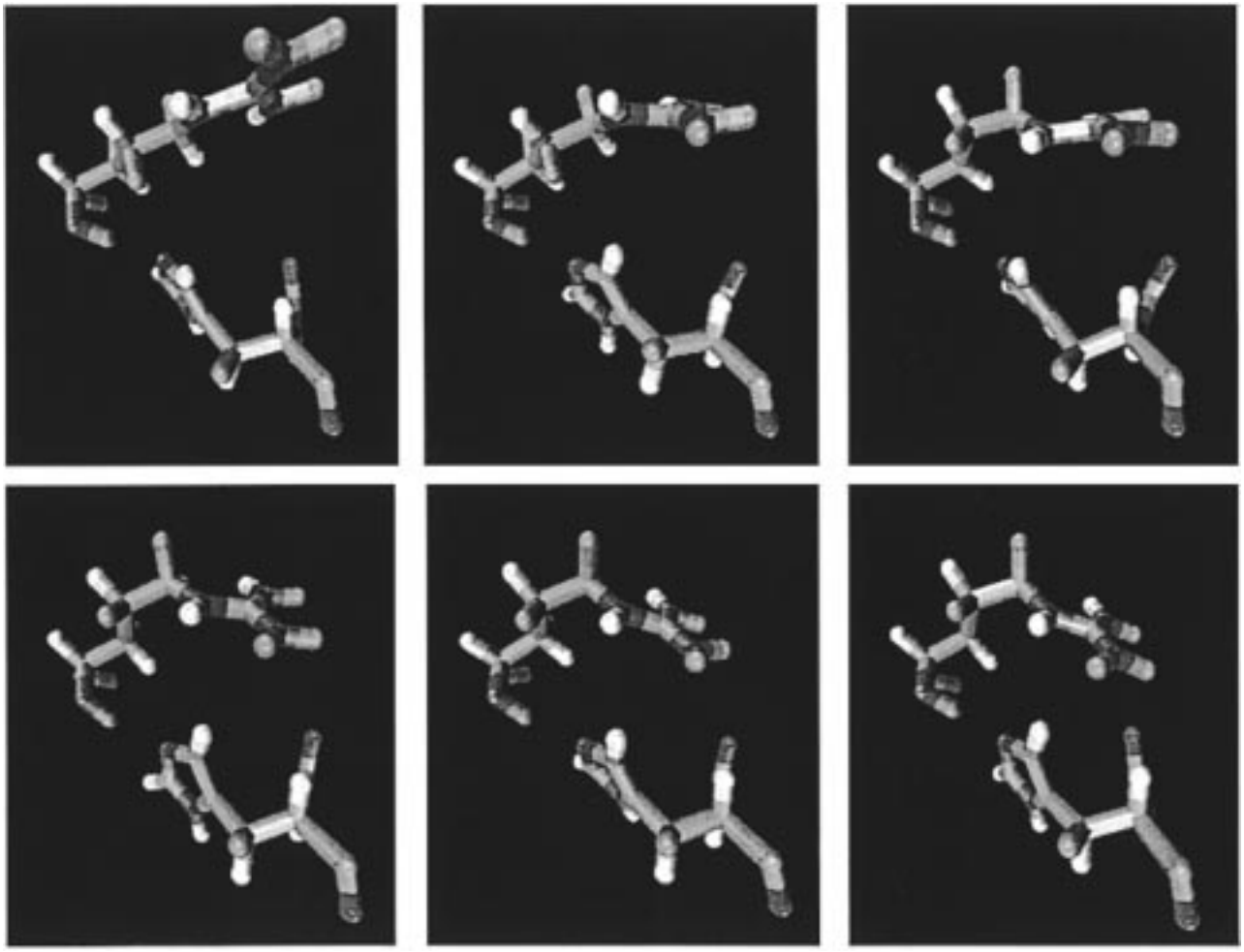

Figure 10. Six snapshots from the simulation to illustrate how the side chain of Arg168-folds back onto the protein to form a H-bond with the backbone oxygen of Ser147. Such a folded conformation is adopted in all other published GFP crystal structures. Snapshots (from left to right in the top and bottom row) are taken at 312 ps (Arg168 side chain exposed to solvent), 318.2 ps, 318.3 ps, 318.4 ps (bond isomerization in Arg168 side chain), 320 ps (H-bond with Ser147:O preformed), and at 328 ps (H-bond with Ser147:O tightly formed). The pictures were generated with VMD.[35]

Some mutants in this interface region have been reported in the literature, e.g., I167T and I167V,[31] that affect GFP's fluorescence signal. We feel that the protein region as shown in Figure 2 may be an excellent target for rational structure-based protein engineering to alter protein thermostability, folding characteristics, and pH sensitivity of GFP.

A very interesting event was observed roughly after the first third of simulation time when Arg168 folded back onto the protein surface. Full formation of the H-bond required ca. 10 ps. The formation of this H-bond certainly stabilizes the connectivity between strands 7 and 8. We speculate that this may be one of the last events in the formation of the protein barrel upon folding of the protein. Mutations of this Arg residue could well affect the formation of actively folded protein. We are not aware of mutational studies of this residue to date.

In conclusion, our results strongly support the picture obtained from crystallographic studies of GFP [7] that GFP is a remarkably stiff protein. Methods of protein engineering, biophysics, and physical chemistry together will enable us to further understand and re-engineer GFP's properties in a predictable fashion, and protein engineering will be facilitated by the stable framework of the GFP architecture.

Acknowledgment. We thank Gert Vriend for the provision of his WHATIF program, Daan van Aalten for help with the WHATIF analysis tools, and Roger Tsien and Jim Remington for helpful discussions. Thanks are also due to Willy Wriggers for valuable comments on the manuscript. This work was in part supported by NSF. Computer time was provided by a grant from the San Diego Supercomputer Center and by the NSF Metacenter Program. V.H. acknowledges a postdoctoral fellowship from NATO through the Deutscher Akademischer Austauschdienst. V.H. was also a fellow of the Program in Mathematics and Molecular Biology and of the La Jolla Interfaces in Sciences Program. NWChem, A Computational Chemistry Package for Parallel Computers, Version 3.0 (1997) was developed by the High Performance Computational Chemistry Group, William R. Wiley Environmental Molecular Sciences Laboratory, Pacific Northwest National Laboratory, and funded by the Offices of Biological and Environmental Research, Computational and Technology Research, and Basic Energy Sciences in the U.S. Department of Energy.

References and Notes

(1) Misteli, T.; Spector, D. L. *Nat. Biotechnol.* **1997**, *15*, 961.
(2) Yang, F.; Moss, L. G.; Phillips, G. N., Jr. *Nat. Biotechnol.* **1996**, *14*, 1246.
(3) Ormö, M.; Cubitt, A. B.; Kallio, K.; Gross, L. A.; Tsien, R. Y.; Remington, S. J. *Science* **1996**, *273*, 1392.
(4) Cody, C. W.; Prasher, D. C.; Westler, W. M.; Prendergast, F. G.; Ward, W. W. *Biochemistry* **1993**, *32*, 1212.
(5) Reid, B. G.; Flynn, G. C. *Biochemistry* **1997**, *36*, 6786.
(6) Rao, B. D. N.; Kemple, M. D.; Prendergast, F. D. *Biophys. J.* **1980**, *32*, 630.
(7) Phillips, G. N., Jr. *Curr. Opin. Struct. Biol.* **1997**, *7*, 821.
(8) Darden, T.; York, D.; Pedersen, L. *J. Chem. Phys.* **1993**, *98*, 10089.
(9) Brejc, K.; Sixma, T. K.; Kitts, P. A.; Kain, S. R.; Tsien, R. Y.; Ormö, M.; Remington, S. J. *Proc. Natl. Acad. Sci. U.S.A.* **1997**, *94*, 2306.
(10) Hooft, R. W. W.; Sander, C.; Vriend, G. *Proteins* **1996**, *26*, 363.
(11) Vriend, G. *J. Mol. Graph.* **1990**, *8*, 52.
(12) *Insight II*, 97.0 ed.; Molecular Simulations Inc.: San Diego, 1997.
(13) Goodford, P. J. *J. Med. Chem.* **1985**, *28*, 849.
(14) Schmidt, M. W.; Baldridge, K. K.; Boatz, J. A.; Elbert, S. T.; Gordon, M. S.; Jensen, J. H.; Koseki, S.; Matsunaga, N.; Nguyen, K. A.; Su, S. J.; Windus, T. L.; Dupuis, M.; Montgomery, J. A. *J. Comput. Chem.* **1993**, *14*, 1347.
(15) Helms, V.; Hom, E. F. Y.; Straatsma, T. P.; McCammon, J. A.; Langhoff, P. *ACS Symp. Ser.* **1998**, *712*, p. 288−295.
(16) Breneman, C.; Wiberg, K. B. *J. Comput. Chem.* **1990**, *11*, 361.
(17) Cornell, W. D.; Cieplak, P.; Bayly, C. I.; Gould, I. R.; Merz, K. M.; Ferguson, D. M.; Spellmeyer, D. E.; Fox, T.; Caldwell, J. W.; Kollman, P. A. *J. Am. Chem. Soc.* **1995**, *117*, 5179.
(18) Anchell, J.; Apra, E.; Bernholt, D.; Borowski, P.; Clark, T.; Clerc, D.; Dachsel, H.; Deegan, M.; Dupuis, M.; Dyall, K.; Fann, G.; Fruchtl, H.; Gutowski, M.; Harrison, R.; Hess, A.; Jaffe, J.; Kendall, R.; Kobayashi, R.; Kutteh, R.; Lin, Z.; Littlefield, R.; Long, X.; Meng, B.; Nichols, J.; Nieplocha, J.; Rendall, A.; Stave, M.; Straatsma, T. P.; Taylor, H.; Thomas, G.; Wolinski, K.; Wong, A. *NWChem, A Computational Chemistry Package for Parallel Computers*, Version 3.0; Pacific Northwest National Laboratory, Richland, WA 99352-0999, 1997.
(19) Ryckaert, J. P.; Ciccotti, G.; Berendsen, H. J. C. *J. Comput. Phys.* **1977**, *23*, 327.
(20) Berendsen, H. J. C.; Postma, J. P. M.; van Gunsteren, W. V.; DiNola, A.; Haak, J. R. *J. Chem. Phys.* **1984**, *81*, 3684.
(21) Amadei, A.; Linssen, A. B.; Berendsen, H. J. *Proteins* **1993**, *17*, 412.
(22) Bertolini, D.; Tani, A. *Phys. Rev. E* **1997**, *56*, 4135.
(23) Angell, C. A. In *Water, A Comprehensive Treatise*; Frank, F., Ed.; Plenum: New York, 1982; Vol. 7.
(24) van Gunsteren, W. F.; Hünenberger, P. H.; Mark, A. E.; Smith, P. E.; Tironi, I. G. *Comput. Phys. Comm.* **1995**, *91*, 305.
(25) Dopf, J.; Horiagon, T. M. *Gene* **1996**, *173*, 39.
(26) Fox, T.; Kollman, P. A. *Proteins* **1996**, *2*, 315.
(27) Niwa, H.; Inouye, S.; Hirano, T.; Matsuno, T.; Kojima, S.; Kubota, M.; Ohashi, M.; Tsuji, F. I. *Proc. Natl. Acad. Sci. U.S.A.* **1996**, *93*, 13617.
(28) Palm, G. J.; Zdanov, A.; Gaitanaris, G. A.; Stauber, R.; Pavlakis, G. N.; Wlodawer, A. *Nat. Struct. Biol.* **1997**, *4*, 361.
(29) Ward, W. W.; Cody, C. W.; Hart, R. C.; Cornier, M. J. *Photochem. Photobiol.* **1980**, *31*, 611.
(30) Kneen, M.; Farinas, J.; Li, Y.; Verkman, A. S. *Biophys. J.* **1998**, *74*, 1591.
(31) Heim, R.; Prasher, D.; Tsien, R. *Proc. Natl. Acad. Sci. U.S.A.* **1994**, *91*, 12501.
(32) Kraulis, P. J. *J. Appl. Crystallogr.* **1991**, *24*, 946.
(33) Ferrin, T. E.; Huang, C. C.; Jarvis, L. E.; Langridge, R. *J. Mol. Graph.* **1988**, *6*, 13.
(34) Huang, E. F. P.; Klein, T. E.; Ferrin, T. E.; Langridge, R. *J. Mol. Graph.* **1991**, *9*, 230.
(35) Humphrey, W. F.; Dalke, A.; Schulten, K. *J. Mol. Graph.* **1996**, *14*, 33.